Pergamon

Int. J. Solids Structures Vol. 35, No. 12, pp. 1289–1308, 1998

0020-7683/98 $19.00 + .00

PII: S0020-7683(97)00104-2

CLASSIFICATION OF SMEARED CRACK MODELS BASED ON MATERIAL AND STRUCTURAL PROPERTIES

S. WEIHE,† B. KRÖPLIN
Institute for Statics and Dynamics of Aerospace Structures, University of Stuttgart, Pfaffenwaldring 27, D-70550 Stuttgart, Germany
† E-mail: weihe@isd.uni-stuttgart.de

and

R. DE BORST
Faculty of Civil Engineering, Delft University of Technology, P.O. Box 5048, NL-2600 GA Delft, The Netherlands

(*Received* 16 *July* 1996; *in revised form* 27 *March* 1997)

Abstract—The paper presents a classification of existing smeared crack models. A concise characterization of the classical models, i.e. the fixed crack and rotating crack model, with their more advanced successors in the form of the multiple fixed crack and the microplane model, identifies the underlying heuristic assumptions with respect to the orientation of the plane of degradation (POD). Following an analytical derivation, the critical PODs are uniquely identified for primary as well as for subsequent secondary cracking. Their direction is shown to depend solely on the character of the unilateral fracture criterion which is applied at the POD and on the character of the applied loading. The ductility of the response is found to play the key role for the orientation of the PODs in the process of secondary cracking. Therefore, it must be considered an important parameter whenever a specific material formulation for a numerical simulation is selected. The proposed analytical approach encompasses the classical models as physically relevant special cases and provides a smooth transition between them. Thus, the presented adaptive fixed crack model allows for a proper choice with respect to the relevant material characteristics and loading conditions.

1. INTRODUCTION

Continuum mechanics has evolved into a universal tool for describing the behaviour of fluids and solids even under severe conditions. However, strongly localized phenomena still pose a great challenge. In the field of material degradation, failure is associated with the emergence of slip or fracture planes, which may occur in ductile or (quasi-) brittle solids, respectively. As a consequence, it is necessary to embed a *discontinuity* of the strain and/or displacement rates in the *continuum* representation. Two strategies have been developed over the past years to cope with this contradiction: the first is to retain the notion of a continuum and to interpret the localized failure mode as a spatial bifurcation problem in the given nonlinear framework. Since this bifurcation is inevitably synonymous with a change of type of the underlying partial differential equations, regularization methods have to be applied to ensure the well-posedness of the given problem (de Borst *et al.*, 1993). They effectively prevent the occurrence of a sharp discontinuity and keep the zone of localized deformations finite. The alternative approach is to adopt the formation of a discontinuity as a feature and to characterize the behaviour of the solid under consideration by the successive failure of the evolving plane of discontinuity. In the latter case, the continuum description of the solid is augmented in the zone of failure by discontinuous contributions, whereas the remaining part of the structure undergoes deformations according to the constitutive relations for the intact continuum.

Thus, two inherently different approaches have been identified: the first characterizes the failure processes with respect to the global (three-dimensional) continuum. It does not incorporate information (stress/strain measures, state variables) which is directly attributed

to the specific failure mechanisms, e.g. in the given situation the planar failure mode of fracture or slip. This approach is, therefore, often termed *phenomenological*. The alternative philosophy introduces the notion of a dimensionally reduced "subcontinuum" or microlevel, which is closely related to the failure mechanism—in the given case the localized failure mode in a two-dimensional fracture or slip plane. As a consequence, the global behaviour of the material in the undamaged regions is described by the constitutive action of the continuum. In the regions where failure occurs, the constitutive behaviour is characterized by the concatenation of the nonlinear material behaviour (stiffness/strength degradation) on the microlevel and the geometrical transformation between the dimensionally reduced "subcontinuum" and the regular three-dimensional continuum.

The latter approach has been advocated by Mohr (1906), who defined the failure of an internal surface in dependence of the tractions acting on it. This is an extension of Coulomb's (1776) idea and the strength of a material is defined by its cohesion and its pressure-dependent internal friction. The actual form of the fracture criterion, cast into a scalar valued function of the tractions, has been a point of long discussion (Leon, 1935). An impressive review of the sophisticated developments during this period is given by Roš and Eichinger (1949), and by Kupfer (1973).

In early algorithmic applications of fracture as a constitutive phenomenon, the material has been assumed to behave totally brittle, i.e. to exhibit a complete loss of stiffness at the onset of failure [original work of Rashid (1968); Cervenka (1970)]. This leads not only to numerical difficulties (Scanlon, 1971; Lin and Scordelis, 1975), but the stress also exhibits the well-known singularity at the crack tip and the model ceases to be mesh objective (Bažant, 1976), unless energy objective measures are introduced (Bažant and Cedolin, 1979). The stress singularity can be avoided by a successive degradation of the material strength/stiffness, which has been introduced for ductile materials by Dugdale (1960) and Barenblatt (1962). With their inspiring contribution, Hillerborg *et al.* (1976) coined the term *fictitious crack model* with respect to the partly damaged fracture process zone, whose evolution is controlled by the dissipated energy in analogy to the concept of fracture toughness.

Based on the decomposition of the total strains into the contributions of the underlying continuum and the additional inelastic strains due to the fracturing process (Litton, 1976), numerous distinct contributions were made to the smeared crack approach (Bažant and Gambarova, 1980; de Borst and Nauta, 1985; Willam *et al.*, 1987). The analogy of the smeared crack approach to the concepts of elasto-plasticity has been established, both with respect to the theoretical aspects (flow rules, state variables), as well as to the numerical aspects (integration schemes, algorithmic tangent operators). The yield condition is, thereby, no longer correlated to plastic flow, but is interpreted as an abstract failure criterion.

For concrete and other quasi-brittle materials, such as rock, ceramics, sea ice etc., fracture is usually initiated under Mode I conditions (maximum stress criterion). During the process of material degradation and subsequent stress redistribution, shear stresses may occur in the fracture plane. They have a significant influence on the quantitative aspects (energy dissipation) as well as on the qualitative aspects (character of the anisotropy) of the residual material parameters [cf. Weihe (1997)]. The concept of a shear retention factor (Suidan and Schnobrich, 1973) and different strategies to couple the shear behaviour to the degradation of the fracture surface under normal action (Rots and de Borst, 1987; Carol and Prat, 1990; Stankowski, 1990) have been developed to account for the interaction between tensile and shear components of the tractions. A complete mode separation has been obtained by Weihe *et al.* (1994).

The qualitative consequences with respect to the direction of the evolving anisotropy have been accounted for in a variety of models: the fixed crack model (Rashid, 1968); the rotating crack model (Cope *et al.*, 1980) in different formats (Bažant, 1983); the multiple fixed crack model (Litton, 1976; de Borst and Nauta, 1985); and several versions of the microplane model (Bažant, 1984; Carol and Prat, 1990) which is motivated by the original contributions of Taylor (1938) and Batdorf and Budiansky (1949) in the context of polycrystalline metals. These models are still considered to be rather independent from each

other. They usually yield very different results in numerical simulations, as has been pointed out by Willam *et al.* (1987), Rots (1988) and Feenstra (1993).

However, no widely accepted criteria exist that address the applicability of the different approaches under the specific conditions of a given project. Therefore, the choice of a specific model is difficult and requires a high level of experience, since the evolving material anisotropy is entirely dominated by the orientation of the plane of degradation (POD). This contribution aims to identify the significant parameters on which this decision must be based.

To achieve this task, the afore-mentioned classical models will be expressed in a unified terminology, clearly identifying their basic mechanisms and fundamental differences, and the consequences thereof. This will lead to a comprehensive analytical treatment in the framework of the newly proposed adaptive fixed crack model. The overall structural brittleness is found to be essential in selecting the appropriate constitutive formulation. As a result, recommendations for the applicability of the classical models will be made, based on the relevant material parameters and the particular structural context.

2. GENERIC CONCEPTS OF THE SMEARED CRACK APPROACH

2.1. *The plane of degradation (POD)*

The most appealing feature of any smeared crack approach is the introduction of a generic plane of degradation (POD). This is an abstract notion and allows the decomposition of a complex constitutive behaviour into one part due to the physical material behaviour on a reduced space (i.e. the POD), and a second contribution, defined by the appropriate (geometric) transformation. Thus, the smeared crack approach distinguishes between the structural (macroscopic) level and the microphysical level, which is of special relevance to the failure mechanism. In the case of a fracture or slip mechanism, it appears natural to adopt the failure plane as the relevant "subspace", and to define the underlying constitutive relations of these planar failure mechanisms with respect to this POD. The inter-relation between the structural level and the POD is given purely by a transformation. This transformation might be of geometric nature or given by the application of the principle of virtual work.

The overall complexity of the constitutive behaviour is, therefore, divided into the constitutive contributions of all active failure mechanisms on one hand, and their geometrical interaction through the individual transformations on the other hand. If the chosen subspace is physically relevant to the failure mechanism, then the elementary constitutive laws can be formulated very rationally on this micromechanical level. Most of the material parameters will become physically interpretable. Thus, they will possess a clear counterpart in the calibration procedure.

In the context of a finite element analysis, multiple cracks can be initiated and intersect each other. Therefore, the number of possible cracks is not limited *a priori* and a new POD is introduced at a material point whenever a new crack initiation (primary or secondary) is detected during the load history. The corresponding orientation of each POD will be evaluated individually.

2.2. *The embedding procedure*

The evolving discontinuity at the POD either relates to the tangential displacements u_t^{cr} across the surface discontinuity (slip plane) or to a combination of normal and tangential components $[u_n^{cr}, u_t^{cr}]$ of the displacements across the POD (fracture). The resulting displacement jump is introduced into the continuous displacement field via "smearing" out over a characteristic distance h as shown in Fig. 1. If no special provisions are taken, the resulting displacement jump has to be accomplished by the conventional shape functions. The characteristic distance h becomes strongly correlated to the mesh size (Oliver, 1989). More advanced techniques employ enhanced element techniques, e.g. based on a mixed variational principle, in order to partially decouple the characteristic width of the degradation zone h from the element size. Amongst others, Armero and Garikipati (1996) employ the enhanced assumed strain method, and Simo and Oliver (1994) and Larsson and

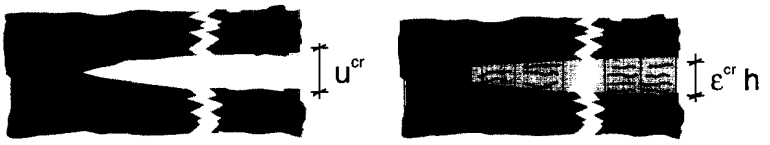

Fig. 1. A topological discontinuity is embedded into a continuum by "smearing" out over a distance h and a decay of the corresponding material parameters.

Runesson (1996) utilize a regularized approximation of the infinitesimal failure zone in an attempt to preserve the localization properties independently of the discretization. Then, the characteristic distance h becomes independent of the size and orientation of the spatial discretization and thus serves as a material parameter only.

In the remaining part of the paper, the "smeared" crack band approach will be utilized, since the classic models are formulated in this framework and an appropriate discussion of the regularization aspects would exceed the objective of this paper, which focuses on a comprehensive comparison of the established smeared crack approaches. Nevertheless, it is emphasized that it is rather straightforward to extend the obtained results to the more advanced embedding technologies.

2.3. *Transformation*: 3-*D continuum* $\rightleftharpoons$ 2-*D plane of degradation*

The overall complexity of the constitutive relations on the structural level is decomposed into the elementary microphysical mechanisms and their geometrical interaction. The structural and microphysical level are related by proper transformations in the kinematic and static measures (Fig. 2). These transformations can either be enforced in a strong sense by a constraint equation or in a weak sense by means of the principle of virtual work.

The constraint (or projection) equations are given in dependence of the directional cosines T_{ij}. They provide the well-known transformation equations between the structural system x and a rotated subsystem $\bar{x}$, which is collinear with the normal to the POD (a Cartesian coordinate system is adopted):

$$\begin{aligned} &\text{static constraint:} && \bar{\sigma}_{ij} := T_{im} T_{jn} \sigma_{mn} \\ &\text{kinematic constraint:} && \bar{\varepsilon}_{ij} := T_{im} T_{jn} \varepsilon_{mn}. \end{aligned} \tag{1}$$

The normal and tangential tractions $[q_n, q_t]$ in the POD (in the rotated coordinate system) and the normal and shear displacements across a POD (smeared over a thickness h) are given by the appropriate components according to the Cauchy theorem:

$$\begin{aligned} &\text{static constraint:} && [q_n, q_{t2}, q_{t3}]^T := [\bar{\sigma}_{11}, \bar{\sigma}_{12}, \bar{\sigma}_{13}]^T \\ &\text{kinematic constraint:} && [u_n, u_{t2}, u_{t3}]^T := h[\bar{\varepsilon}_{11}, 2\bar{\varepsilon}_{12}, 2\bar{\varepsilon}_{13}]^T. \end{aligned} \tag{2}$$

In this conception of a strong form, the components on the microphysical level are connected

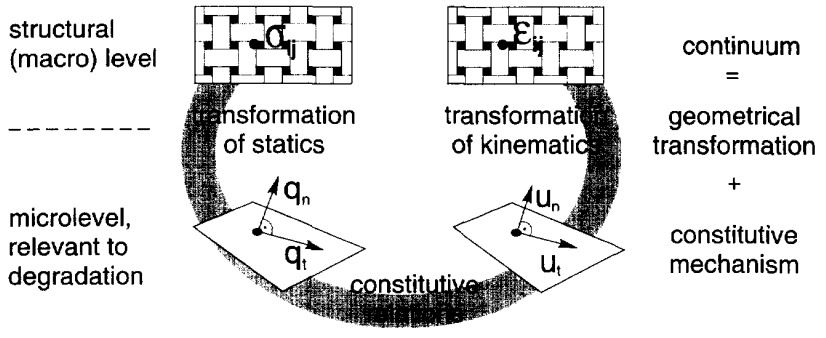

Fig. 2. The structural and micromechanical levels are related by proper transformations in the kinematic and static measures.

uniquely to the continuum stresses (or strains) by the Cauchy projection. Subsequently, an arbitrary, i.e. non-linear, constitutive relationship is applied to obtain the dual strains (or stresses) on the microphysical level. These local dual variables, however, do not in general fulfill the corresponding dual constraint in the strong form, since the strong form of back-transformation would not provide a unique macroscopic dual field. Thus, it is necessary to introduce the weak form of the dual constraint (Bažant, 1984) to finally transfer the dual variables back to the continuum level in an energetically consistent manner:

$$\int_V \sigma_{ij}\delta\varepsilon_{ij} := \int_\Omega \frac{1}{h} q_k \delta u_k \quad \text{for all local measures } q_k, u_k. \tag{3}$$

V and Ω denote the volume and the surface, respectively, of an (infinitesimal) control sphere at a material point. Since the local dual measures (stress or strain) fulfill the constraint equation only in an integral (weak) sense and do not satisfy the corresponding projection condition, they possess no direct physical meaning and become rather fictitious.

In the preceding section, the overall constitutive response has been subdivided into a part due to physical action and another, which is due to purely geometrical effects. Along this argumentation, it is straightforward to assume that the physical response is comprised by a regular part due to the underlying (undamaged) continuum and a second part, which is activated during failure and describes the degradation phenomena. Thus, the total response on the structural level is formulated as a function of the virgin continuum, enriched by the microphysical degradation effects which are expressed on the individual PODs and transformed onto the structural level via a geometrical transformation. For the hypothesis of a linear elastic (isotropic) behaviour of the virgin material and a degradation mechanism which can be described by inelastic strain components this translates into

$$\begin{aligned} \boldsymbol{\varepsilon} &= \left(\boldsymbol{\varepsilon}^{\mathrm{co}} + \sum_k \frac{1}{h_k} \mathbf{N}_k \mathbf{u}_k^{\mathrm{cr}}\right) \\ \boldsymbol{\sigma} &= \mathbf{D}^{\mathrm{co}}\boldsymbol{\varepsilon}^{\mathrm{co}} = \mathbf{D}^{\mathrm{co}}\left(\boldsymbol{\varepsilon} - \sum_k \frac{1}{h_k} \mathbf{N}_k \mathbf{u}_k^{\mathrm{cr}}\right) \end{aligned} \tag{4}$$

where $\boldsymbol{\varepsilon}^{\mathrm{co}}$ denotes the elastic strains of the continuum and $\mathbf{N}_k$ the transformation matrix for the inelastic relative displacements $\mathbf{u}_k^{\mathrm{cr}}$ of each activated crack k. Here, the strong version of the constraint equations can be enforced for the stresses and the inelastic strains, since the stress depends on the elastic strains only. Thus, the microphysically activated inelastic strains do not (directly) alter the stresses and, therefore, the stress consistency via the elastic strains is preserved.

2.4. *Constitutive assumptions on the microphysical level*

2.4.1. *Initiation of failure.* All variables which may eventually become relevant for the initiation and evolution of the material degradation are available at the POD, either through the above mentioned transformations, or since they are defined directly at the microphysical level. As a consequence, most of the common failure criteria can be applied at the POD: classical damage mechanics as a function of the accumulated total strains (Carol *et al.*, 1992) can be used as well as fracture mechanics on the basis of critical energy release rates (Rinderknecht, 1994). However, in most applications, stress based failure criteria have been employed. The degradation is then often realized by inelastic deformations in the sense of a relaxation process. As it will be shown in the following section, the redistribution of stresses and a subsequent rotation of the principal stress and strain axes inevitably leads to combined normal/shear loading on the POD, and the constitutive relations must provide for a proper mode separation. Without loss of generality, the explicit formulae will be derived for a specific constitutive model. Since the model itself is not the subject of the

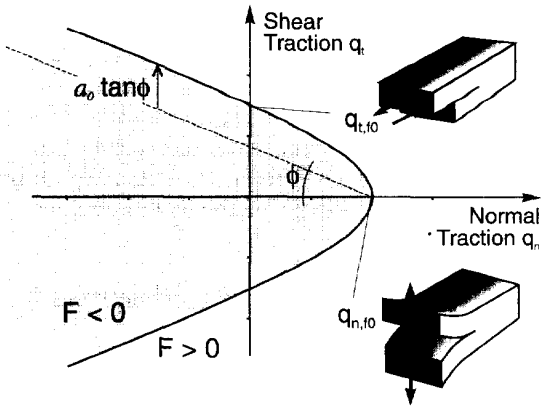

Fig. 3. Crack initiation is determined by the fracture criterion.

present discussion, only a short outline will be given. For a detailed description, the reader is referred to Weihe (1995).

The critical stress state is characterized by the negative to positive transition of the scalar valued failure criterion F, which is depicted in Fig. 3. For simplicity, a two-dimensional continuum under plane stress or plane strain conditions is considered (and, therefore, the POD reduces to a one-dimensional line):

$$F := -(q_n - q_{n,f} - a)^2 + \frac{q_t^2}{\tan^2 \phi} + a^2 \stackrel{!}{=} 0. \tag{5}$$

The material parameters are:

$q_{n,f}$ describes the tensile strength of the POD under vanishing shear stresses (Mode I conditions). As it will be shown subsequently, this microphysical tensile strength of the POD not necessarily coincides with the uniaxial strength of the material at the structural level.

a characterizes the influence of the asperities and the roughness of the evolving surface. It provides further shear resistance in addition to the portion, which is already provided by pure internal friction. The intensity of the asperities is strongly dependent on the tangential slip on the POD.

$\tan\phi$ corresponds to the internal angle of dry friction in the sense of Mohr–Coulomb. It characterizes the linear dependence of the residual shear resistance with respect to the applied normal compression after complete loss of cohesion in the final state of the surface roughness.

The initial value for the asperity parameter a_0 (the index 0 denotes the value in the undamaged state) is calibrated from the initial microphysical shear strength of the POD (which again need not coincide with the shear strength of the continuum):

$$F|_{q_t = 0} \stackrel{!}{=} 0 \overset{(5)}{\Rightarrow} q_{t,f} = \tan\phi \sqrt{q_{n,f}^2 + 2aq_{n,f}}. \tag{6}$$

For subsequent qualitative reasonings, the (microphysical) relative shear strength γ_0 in the undamaged state is introduced:

$$\gamma_0 := \frac{q_{t,f0}}{q_{n,f0}}. \tag{7}$$

Thus, eqn (6) can be rewritten as

$$a_0 = \frac{1}{2} q_{n,f0} \left(\left(\frac{\gamma_0}{\tan \phi} \right)^2 - 1 \right) \geqslant 0 \rightsquigarrow \gamma_0 \geqslant \tan \phi. \tag{8}$$

2.4.2. *Evolution of failure.* The degradation of the PODs is modelled by inelastic deformations. Analogous to classical flow theory of plasticity, the inelastic velocities $\dot{\mathbf{u}}_k^{\mathrm{cr}} = [\dot{u}_n^{\mathrm{cr}}, \dot{u}_t^{\mathrm{cr}}]_k$ across a POD are formulated according to a "flow" rule

$$\begin{aligned} \dot{\mathbf{u}}^{\mathrm{cr}} &= \dot{\lambda} \mathbf{m}, \quad \mathbf{m} := \mathbf{A} \frac{\partial F}{\partial \mathbf{q}} \\ F &\leqslant 0, \quad \dot{\lambda} \geqslant 0, \quad F \dot{\lambda} = 0 \end{aligned} \tag{9}$$

where the transformation matrix $\mathbf{A}$ is introduced to provide for a pressure dependent dilatation:

$$\begin{aligned} \mathbf{A} &:= \begin{bmatrix} \eta & 0 \\ 0 & 1 \end{bmatrix}, \quad \eta := \eta_1 \exp\left(-\eta_0 \frac{q_{t,r}}{q_{n,f0}} \right) \\ q_{t,r} &:= \begin{cases} 0, & q_n \geqslant 0 \\ -q_n \tan \phi, & q_n < 0 \end{cases} \end{aligned} \tag{10}$$

η_0 realizes a decreasing dilatation with increasing normal compressive stress on the POD. Therefore, the dilatation is asymptotically suppressed under high confining stresses. A constant reduction of the dilatation effect is provided by η_1, which is activated for compressive as well as for tensile normal tractions on the POD.

In analogy to fracture mechanics, a complete separation of the POD is achieved when the dissipated energy equals a material constant, namely the fracture toughness G_f with respect to the individual failure Modes I and II. Assuring that the energy which is dissipated due to friction is excluded, this transforms into:

$$\begin{aligned} G_f^{\mathrm{I}} &:= \int_{u_n^{\mathrm{cr}}=0}^{\infty} q_n \, \mathrm{d}u_n^{\mathrm{cr}} \Big|_{\substack{q_t = 0 \\ \mathrm{d}u_n^{\mathrm{cr}} > 0}} \\ G_f^{\mathrm{II}} &:= \int_{u_t^{\mathrm{cr}}=0}^{\infty} (|q_t| - q_{t,r})| \, \mathrm{d}u_t^{\mathrm{cr}}| \Big|_{q_n = 0} \quad \text{with } q_{t,r}\Big|_{q_n=0} = 0. \end{aligned} \tag{11}$$

The energy dissipated during the degradation process, separated with respect to the failure mode and normalized with respect to the specific fracture toughness, is used to formulate the internal state variables ξ_k which are evaluated individually for each activated POD_k:

$$\begin{aligned} \dot{\xi}^{\mathrm{I}} &:= \begin{cases} \dfrac{1}{G_f^{\mathrm{I}}} q_n \dot{u}_n^{\mathrm{cr}} & \dot{u}_n^{\mathrm{cr}} \geqslant 0 \\ 0 & \dot{u}_n^{\mathrm{cr}} < 0 \end{cases} \\ \dot{\xi}^{\mathrm{II}} &:= \frac{1}{G_f^{\mathrm{II}}} (|q_t| - q_{t,r}) |\dot{u}_t^{\mathrm{cr}}|. \end{aligned} \tag{12}$$

Since any slip or fracture event is uniquely correlated to a specific POD, the history of the degradation mechanisms are described individually by the state variables ξ_k of the corresponding POD_k.

The current residual strength of each activated POD is evaluated individually according to the following assumptions:

- Mode I failure leads to a complete decohesion and thus successively reduces the microphysical tensile strength $q_{n,f}$ to zero. However, fracture under Mode I will not reduce the roughness of the surface and thus, the asperity parameter a remains constant.
- Mode II failure decreases the tensile strength and grinds off the asperities as well. Therefore, shear failure affects both the tensile strength $q_{n,f}$ and the asperity parameter a, again evaluated individually for each POD:

$$q_{n,f} = (1-\kappa_n)q_{n,f0}, \quad \kappa_n := \min(1, \xi^{\mathrm{I}} + \xi^{\mathrm{II}})$$
$$a = (1-\kappa_a)a_0, \quad \kappa_a := \xi^{\mathrm{II}}. \tag{13}$$

- Mixed mode failure evolves as a combination of both generic failure modes. It is automatically achieved by activating both state variables during the degradation process. However, the specific contributions due to Modes I and II can be distinguished by the values of ξ^{I} and ξ^{II}, respectively.

The residual shape of the fracture criterion is not unique, but depends on the load history as shown in Fig. 4. Introducing eqns (13) via eqn (6) into the differential equations (12) yields after integration the corresponding evolution of the local tensile and shear strength:

$$q_{n,f} = q_{n,f0} \exp\left(-\frac{q_{n,f0}}{G_f^{\mathrm{I}}} u_n^{\mathrm{cr}}\right) \quad \text{under Mode I}$$
$$q_{t,f} = q_{t,f0} \exp\left(-\frac{q_{t,f0}}{G_f^{\mathrm{II}}} u_t^{\mathrm{cr}}\right) \quad \text{under Mode II.} \tag{14}$$

It is noted that not only the tensile strength is reduced exponentially with respect to the normal relative displacement under Mode I, but also the shear strength is an exponentially decreasing function of the corresponding relative shear displacement under Mode II conditions.

2.5. *Corrolar: individuality and interaction of the PODs*

At a single point in space, multiple cracks or slip planes may become active under different orientations. It is assumed that the degradation of a certain POD via inelastic relative displacements contributes only to the internal state variables of this particular POD, i.e. they do not augment the degradation of other mechanisms that might be active in the same material point as well. Thus, the presented constitutive relations adopt the concept of locality in an orientational sense.

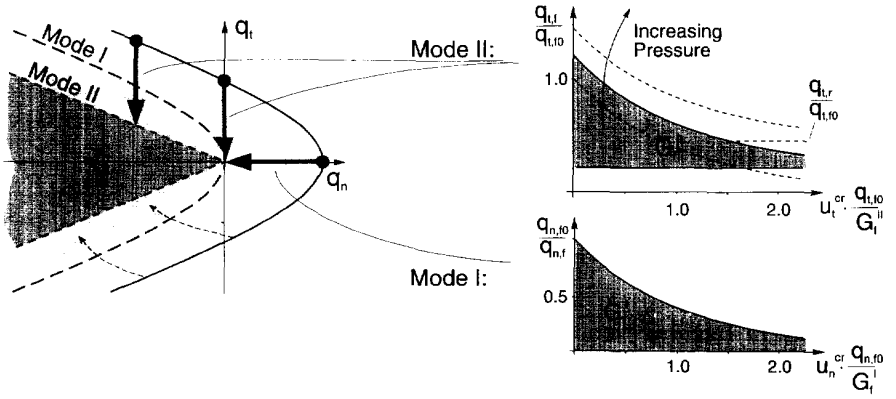

Fig. 4. Shape of the residual fracture criterion, which is dependent on the load history (left). The corresponding evolution of the microphysical shear strength for different pressure levels (top) and the microphysical tensile strength (bottom).

However, it has been stated above that the microphysical stress and inelastic strain measures will be consistent in a strong form with the continuum fields. If the applied stress state activates nonlinear displacement components $\dot{\mathbf{u}}_k^{cr}$ in a specific POD_k, then the microphysical degradation of this POD_k will be reflected via the kinematic constraint in a relaxation of the corresponding continuum stress state $\boldsymbol{\sigma}$. Due to the static constraint, which is enforced at all times, the relaxation of the continuum stress state will be reflected at each $POD_{i \neq k}$ (in this material point) as well. Crack shielding is herewith inherently present in the model. It will become an important failure in the example, which is presented in the next section.

3. THE CLASSICAL MODELS REVISITED

In the previous section, a constitutive model has been defined under the assumption that the orientation of the POD is known. Thus, the model is well defined for an *a priori* defined fracture plane as it exists for example at a bimaterial interface or under symmetric geometrical and loading conditions. However, when the failure region is not prescribed, additional information—namely the orientation of the POD—has to be evaluated. In this section, some of the classical models with their underlying assumptions with respect to the orientation of the POD will be discussed. Based on these findings, a new approach with distinct advantages over the classical models will be presented.

- In the fixed crack model (FCM), initially proposed by Rashid in 1968, failure is initiated perpendicular to the maximum tensile (principal) stress when the principal stress exceeds the uniaxial tensile strength f_t' of the continuum. f_t' is assumed to be identical to the microphysical tensile strength $q_{n,f0}$ of the POD. Thus, the critical failure state is supposed to occur under pure Mode I conditions, and the crack is initiated in the apex of the initial fracture criterion F_0. The interaction capacity of tensile and shear tractions, as it is expressed e.g. in eqn (5), is completely neglected. In the process of further loading, the initial orientation of the POD is maintained fixed. This is in accordance with the physical understanding of a crack, which, after initiation, possesses a fixed direction with respect to the material. Secondary cracking is not accounted for, and thus, non-proportional loading can result in shear and normal stresses parallel to the initial crack which exceed the uniaxial strength significantly. Several strategies have been proposed to incorporate degradation mechanism for these evolving shear stresses: a decreasing shear retention factor, a direct coupling of the shear strength to the crack opening displacement u_n^{cr}, and softening behaviour which incorporates the shear components as well [see Weihe (1995)]. Nevertheless, in structural problems, the FCM tends to overestimate the experimental failure load.
- The rotating crack model (RCM, Cope *et al.*, 1980) assumes the initiation of the degradation to be controlled by the maximum tensile stress as well. In the failure evolution, however, the orientation of the failure mechanism (i.e. the material anisotropy) is adjusted to remain orthogonal to the direction of the current major principal stress, where it is assumed that the axes of principal stress coincide with the axes of principal strain (Bažant, 1983). As a consequence of the rotation of the POD, the POD experiences only normal traction components q_n. The shear traction q_t is identically zero. Thus, the degradation mechanism is solely controlled by the major principal stress and the results become equivalent to a material formulation which is based on stress invariants. The RCM eventually performs very similar to isotropic plasticity, e.g. the Rankine criterion (Feenstra and de Borst, 1995). In a structural context, the RCM reacts much more ductile when compared to the FCM. This is the result of two phenomena, which are correlated to the adaption of the failure mechanism to the current loading direction: the failure mechanism is always collinear to the direction of the principal loading and, thus, the major stress component is most affected by the relaxation process. At the same time, the energy dissipation is maximized and the rate of softening becomes very high.
- The multiple fixed crack model (MFCM) retains the physical plausibility of the FCM. It circumvents the artificial stiffness of the FCM by allowing for the formation of

secondary crack(s). Once they have been initiated, all existing cracks remain fixed in their initial orientation. The primary crack is initiated analogous to the FCM, usually under the assumption of a maximum stress criterion. Secondary cracks are activated, when the principal stress has rotated significantly from the direction of the previously activated cracks, where the threshold angle is a predefined material parameter $\Delta\alpha^{Th}$. In the work of de Borst and Nauta (1985), it is further required that the fracture criterion is violated in order to initiate a new crack. If this assumption is adopted as well, the MFCM is conceptually very similar to the microplane model, which will be discussed below in detail.

An alternative version of the MFCM has been proposed by Rots (1988), where a significant rotation of the principal loading axis is assumed to be sufficient in order to rotate the crack. In this framework, the MFCM provides a transition between the FCM ($\Delta\alpha^{Th} = 90^\circ$) and the RCM ($\Delta\alpha^{Th} \to 0^\circ$). The computational results will strongly depend on the actual value of the threshold angle. The choice of the threshold angle, however, cannot be made on the basis of any calibration procedure, but has to be selected by the analyst.

- As early as 1938, Taylor interpreted the complex macroscopical behaviour of polycrystalline metals as the interaction of distinct slip planes, which are due to the inner molecular structure of the material. Bažant (1984) and coworkers (Carol and Prat, 1990) transferred this perception of microscopically inhomogeneous media in the context of the microplane model (MPM). It is postulated that the overall behaviour of a degrading material can be described by evaluating a finite number of representative microplanes. Their orientation is defined *a priori* in the sense of discrete sample directions, which is quite analogous to sample (integration) points in (discretized) finite elements.

  In the case of the microplane model with a static constraint in the strong sense [cf. eqn (1)], predefined failure planes are activated as soon as the loading exceeds the critical value, which is characterized by the fracture criterion. This is evaluated independently for all sample PODs and, therefore, no special provisions have to be taken for secondary cracking. Primary and secondary cracks are initiated not necessarily under Mode I. In fact, any combination of tensile and shear components of the tractions which violates the fracture criterion leads to mixed mode failure.

  The microplane models which enforce the static constraint in the weak sense only, are fundamentally different from the smeared crack models, and hence will not be discussed in this paper.

It can be concluded that two aspects of the smeared crack approach are realized in a different manner by the classical models:

- The crack initiation in relation to the applied load is based on the hypothesis of the maximum stress assumption or is dependent on predefined sample directions.
- The response to further (non-proportional) loading leads either to a rotation of the POD or the initiation of secondary (and possibly further) cracks.

These underlying assumptions of the classical models are fundamentally different from each other, and the numerical results reflect a significant bias due to these specific assumptions. However, the orientation of primary and secondary cracks are characteristic for a specific material and should not be dependent on specific assumptions of the model. In the following, an analytical treatment of the crack initiation will be presented, and the material parameters which are relevant for the crack orientation will be identified.

4. THE ADAPTIVE FIXED CRACK MODEL (AFCM)

The material is assumed to be isotropic in the initial undamaged state. Therefore, the fracture criterion F_0 is valid for any orientation of the potential POD, and the critical state is given by $F_0 = 0$.

$$F_0|_\alpha \equiv F_0 \ \forall\ \alpha \in [0°, 180°] \text{ symmetric.} \tag{15}$$

The local tractions $[q_n, q_t]$ on the POD are given by the static constraint (1). They are expressed as a function of the major and minor principal stresses $[\sigma_I, \sigma_{II}]$ in the (two-dimensional) continuum and the angle α between the normal to the POD and the direction of the major principal stress.

$$\begin{aligned} q_n &= \sigma_I \cos^2 \alpha + \sigma_{II} \sin^2 \alpha \\ q_t &= \frac{\sigma_I - \sigma_{II}}{2} \sin(2\alpha). \end{aligned} \tag{16}$$

In order to take into account the evolution of the loading process, the load-type parameter ζ is introduced. It characterizes the *loading state of the continuum* and is constant during incrementally proportional loading.

$$\zeta := \frac{\sigma_I + \sigma_{II}}{\sigma_I - \sigma_{II}}. \tag{17}$$

The following specific loading states are readily verified:

$$\begin{aligned} \zeta &\to -\infty && \text{equibiaxial compression} \\ \zeta &= -1 && \text{uniaxial compression} \\ \zeta &= 0 && \text{pure shear} \\ \zeta &= 1 && \text{uniaxial tension} \\ \zeta &\to \infty && \text{equibiaxial tension.} \end{aligned} \tag{18}$$

Expression (17) is introduced into Mohr's transformation rules (16). Thus, the evolution of the microphysical tractions is obtained in dependence of the angle α of the POD and the load-type ζ of the applied loading. If this relation is introduced into the fracture criterion F_0, then the critical POD can be characterized uniquely:

$$F_0(\zeta, \alpha) \leqslant 0, \quad \alpha_{crit} = \{\alpha \,|\, F_0(\zeta, \alpha) \stackrel{!}{=} \max\}. \tag{19}$$

The critical orientation α_{crit} maximizes the fracture criterion, and the corresponding critical loading state $\boldsymbol{\sigma}_{crit}$ fulfills the initiation condition $F_0|_{\alpha_{crit}} = 0$. This situation is depicted in Fig. 5.

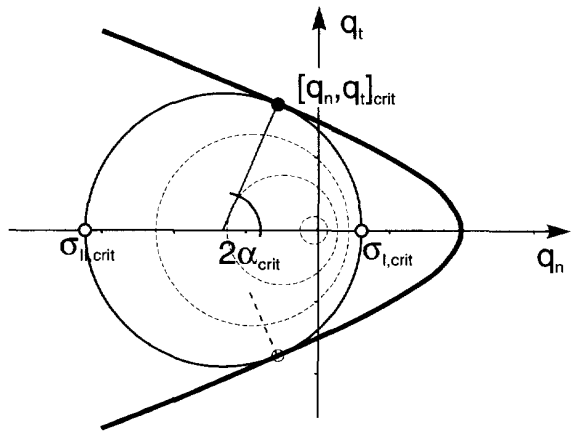

Fig. 5. The analytical determination of the orientation of the critical POD α_{crit}.

The approach outlined above is independent of the specific algebraic format of the fraction criterion. The critical direction for smeared crack models can be expressed in general as a function of the loading ζ and the material parameters $\mathscr{X}$ of the fracture criterion:

$$\alpha_{\text{crit}} = \alpha_{\text{crit}}(\zeta, \mathscr{X}) \quad \text{for any fracture criterion } F_0(\mathscr{X}). \tag{20}$$

For the specific fracture criterion, which has been presented in eqn (5), the orientation of the critical POD can be evaluated according to the preceding outline as:

$$\cos(2\alpha_{\text{crit}}) = \frac{\dfrac{\zeta \tan^2\phi}{(1+\tan^2\phi)(\gamma_0^2+\tan^2\phi)}\sqrt{(1+\tan^2\phi)(4\gamma_0^2-(1-\zeta^2)(\gamma_0^2-\tan^2\phi)^2)}-1}{\zeta-\dfrac{1}{\gamma_0^2+\tan^2\phi}\sqrt{(1+\tan^2\phi)(4\gamma_0^2-(1-\zeta^2)(\gamma_0^2-\tan^2\phi)^2)}} \tag{21}$$

with

$$\gamma_0 \overset{(7)}{=} \frac{q_{t,f_0}}{q_{n,f_0}}.$$

It is verified that the critical direction is completely determined by the material parameters of the fracture criterion $F_0(\gamma_0, \phi)$ and the applied loading ζ. Equation (21) has, in general, two solutions. Although activating both, usually only one of them remains active in a structural setting to finally yield a continuous failure propagation through the material.

The stress state $\boldsymbol{\sigma}_{\text{crit}}$ that enters eqn (21) via eqn (17) reflects the current loading and the influence of all active PODs through the static constraint, which is enforced at all times. Furthermore, recalling that any non-damaged POD is characterized by the initial fracture criterion F_0 [eqn (15)], eqn (21) is not only valid to obtain the critical angle for the primary crack. It characterizes the most critical plane at any instant of loading, independent of the number of already active PODs. Thus, a new crack is introduced whenever the initial fracture criterion F_0 is violated under the current critical direction α_{crit}. The inclination between subsequently initiated cracks will depend on the material parameters and the structural response. In this sense, eqn (20) yields a multiple fixed crack approach which adapts to the specific loading history.

4.1. *Evaluation of the local mode of fracture*

The angle α_{crit} describes the orientation of the critical POD with respect to the major principal stress and indicates the failure mode. Under Mode I, the POD is perpendicular to the major principal stress

$$\text{Failure under Mode I} \Leftrightarrow \alpha_{\text{crit}} = 0^\circ \tag{22}$$

which, using eqn (21), results in the following necessary condition for Mode I failure (sufficient together with the condition $F_0|_{\alpha_{\text{crit}}} \geqslant 0$):

$$\alpha_{\text{crit}} = 0^\circ \Leftrightarrow 0 \leqslant 1 - \frac{\zeta - 1}{\zeta + 1} \leqslant \gamma_0^2 - \tan^2\phi. \tag{23}$$

The relevant parameters are again γ_0 and ζ. The left-hand side of the inequality constitutes a bound on the applied loading, whereas the right-hand side characterizes the microphysical strength of the POD. It is seen that

- Mode I failure is feasible for $\zeta > -1$ (necessary condition). Thus, a stress state of pure shear in the continuum ($\zeta = 0$) may lead to a local Mode I failure in the POD.

- If the applied loading is dominated by tensile components ($\zeta \gg 0$), then failure under Mode I is favoured. For pure equibiaxial tension ($\zeta \to \infty$), failure necessarily occurs under Mode I.
- Materials with a low relative shear strength γ_0 usually fail under mixed mode ($\rightsquigarrow$ metals, polymers), whereas materials with a high relative shear strength tend to fail under Mode I ($\rightsquigarrow$ concrete, ceramics).

In conclusion, cracks will occur under Mode I if the material is sufficiently brittle and if the loading is dominated by tensile components. In other cases, e.g. in the neighbourhood of loading platens, the maximum stress criterion for fracture initiation is inadequate, even for brittle materials.

In the compressive regime ($q_n \ll 0$), the fracture criterion F_0 approaches the asymptotic form

$$F_{0,\text{asymp}} := (q_n - q_{n,f_0} - a_0) - \frac{q_t}{\tan\phi} \stackrel{!}{=} 0 \tag{24}$$

and a compressive bound for fracture is established:

$$\left(\frac{\sigma_\text{I} + \sigma_\text{II}}{2} - q_{n,f_0} - a_0\right)\sin\phi \leqslant \frac{\sigma_\text{I} - \sigma_\text{II}}{2} \tag{25}$$

which is reformulated as

$$\zeta \geqslant -\frac{1}{\sin\phi}\left(1 + \frac{q_{n,f_0} + a_0}{\dfrac{\sigma_\text{I} + \sigma_\text{II}}{2}}\right)^{-1}. \tag{26}$$

This relation can be simplified using $\zeta \ll 0$, which leads to $|\sigma_\text{I} + \sigma_\text{II}| \gg q_{n,f_0} + a_0$ and finally:

$$\zeta \geqslant -\frac{1}{\sin\phi}, \quad \zeta \ll 0. \tag{27}$$

Thus, the failure mode of the POD is characterized by the following relations:

$$\begin{array}{ccccc} \text{eqn(27)} & & \text{eqn (21)} & & \text{eqn (23)} \\ \text{compr. bound (no failure)} & \Leftrightarrow & \text{mixed mode} & \Leftrightarrow & \text{Mode I} \end{array}.$$

It can be seen from Fig. 6 that concrete (typically $\gamma_0 \approx 2.0$) will fail in most loading situations

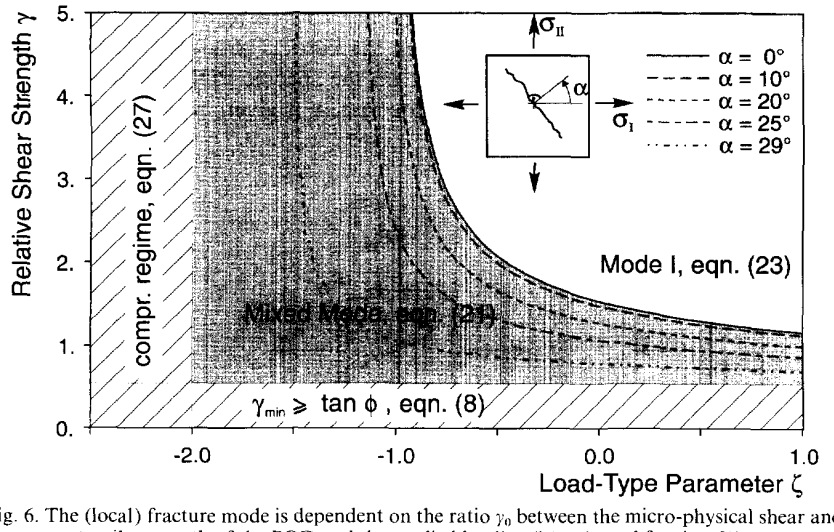

Fig. 6. The (local) fracture mode is dependent on the ratio γ_0 between the micro-physical shear and tensile strength of the POD and the applied loading ζ (evaluated for $\phi = 0°$).

under Mode I, even if a macroscopic shear stress is applied. Significant compressive stresses have to be present, before mixed mode failure can be expected.

The presented adaptive fixed crack model can be used to replace the assumptions of the classical models with respect to primary and secondary crack initiation. An analytical criterion has been presented, and the direction of the critical POD is adaptively determined, based on the current loading situation and the material parameters.

5. EXAMPLE

The "tension–shear" problem (Fig. 7), originally proposed by Willam *et al.* (1987), is used to further illustrate the phenomenon of primary and secondary crack formation and the mechanism of crack shielding. The primary crack in the tension–shear specimen is initiated through uniaxial loading under displacement control. Subsequently, the loading is applied with a continuous rotation of the directions of the principal strains $[\dot{\varepsilon}_{xx} : \dot{\varepsilon}_{yy} : 2\dot{\varepsilon}_{xy}] = [0.50 : 0.75 : 1.00]$.

It is seen from Fig. 8 that, for identical material parameters, the characteristic response differs drastically for the conventional models, cf. Willam *et al.* (1987), Rots (1988), and Feenstra (1993). Since these differences are caused by the fundamentally different assumptions inherent in the models, the various results do not converge to a common solution, and thus the computational predictions are difficult to assess.

All formulations provide an immediate relaxation of the principal stress as the primary crack is initiated. However, the fixed crack model exhibits a steady increase of the stress state as soon as the principal axes of stress rotate significantly against the primary crack. Eventually, the principal stress exceeds indeed the critical strength limit (cf. Section 6). Simultaneously, the shear stress σ_{xy} is steadily increasing. The rotating crack model shows a totally different behaviour: the softening response in the principal stress diagram follows exactly the microphysically prescribed exponential decay and the shear stress σ_{xy} remains bounded. The response of the multiple fixed crack model duplicates the behaviour of the fixed crack model until a secondary crack orientation is activated. The very pronounced relaxation when compared to the microplane model is explained by the transfer of the state variables, from the preciously activated crack to the rotated one, whereas in the microplane model, the microplanes degrade independently from each other. In the final states of loading, the failure in the multiple fixed crack model is accumulated by two active mechanisms. Their alternative activation is reflected in the oscillatory response.

With the adaptive fixed crack approach, the formation of secondary cracks is uniquely defined. The microphysical constitutive history is discussed in detail in Fig. 10. The corresponding five load levels are depicted in Fig. 9.

The initial fracture criterion F_0 and the subsequent shapes of the degradation process are visualized in Fig. 10, where the pictures in each row correspond to a load level from I (top) to V (bottom). The horizontal axis and the vertical axis represent the normal and shear components of the tractions which act on the specific POD. The orientation of the POD with respect to the global x–y-coordinate system is given in the small inserts.

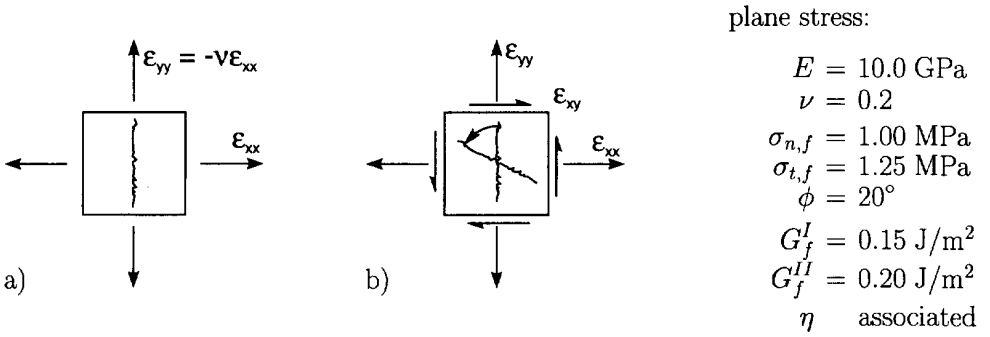

Fig. 7. Tension–shear: loading (a) before and (b) after initial failure.

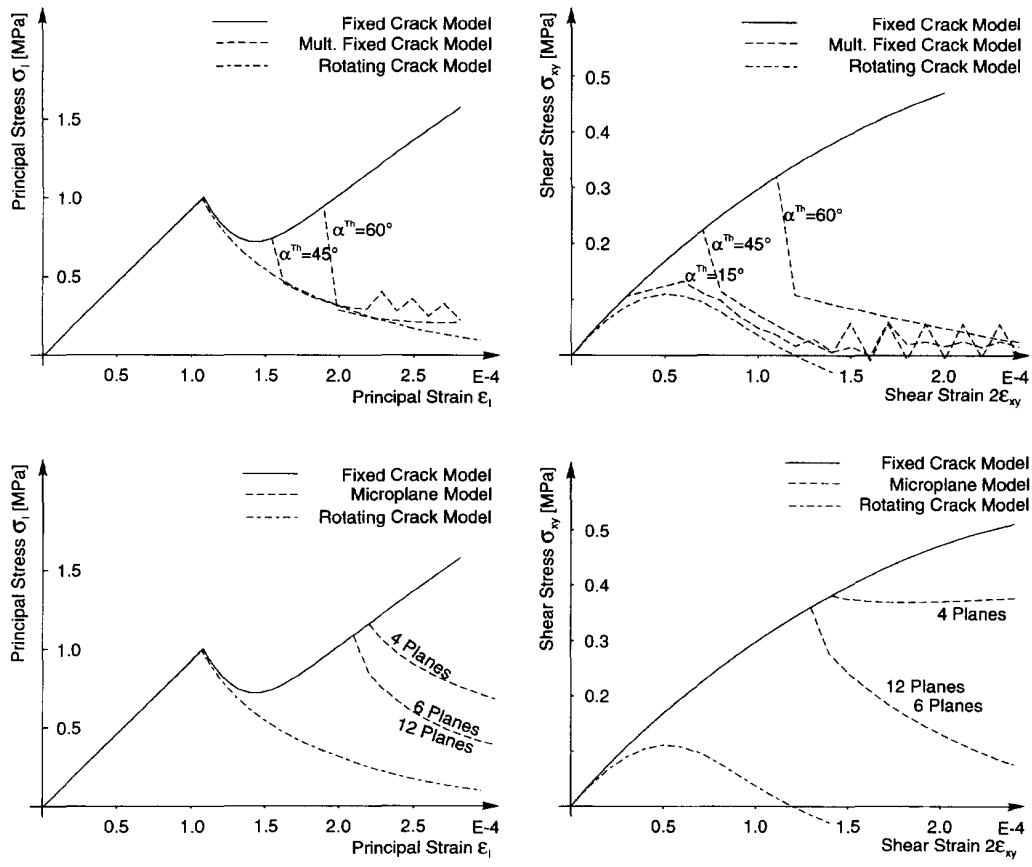

Fig. 8. Response of the classical models to the tension–shear problem.

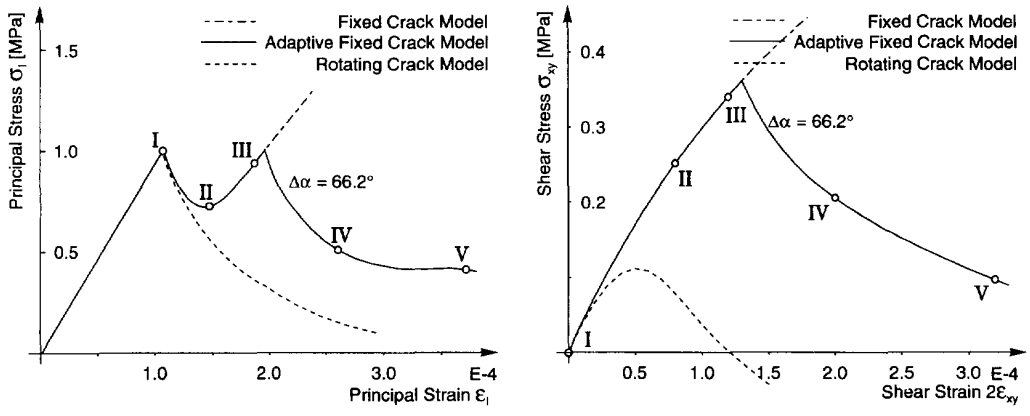

Fig. 9. Response of the adaptive fixed crack model to the tension–shear problem. The loading steps which are discussed in detail in Fig. 10 are marked I–V.

The left-hand column characterizes the currently most critical POD, which is given by eqn (21). The Mohr circle is extrapolated in this (left) column to the critical loading σ_{crit}, for which $F_0|_{\alpha_{\text{crit}}} = 0$. The current tractions are indicated by a small circular mark. The dashed line in the insert shows the current orientation of the major principal stress.

Columns two and three depict the cracks which are subsequently activated. The evolution of the loading surfaces are depicted with dashed lines including the corresponding stress state. The current (softened) fracture criterion is given by the solid line with the appropriate Mohr circle characterizing the current loading.

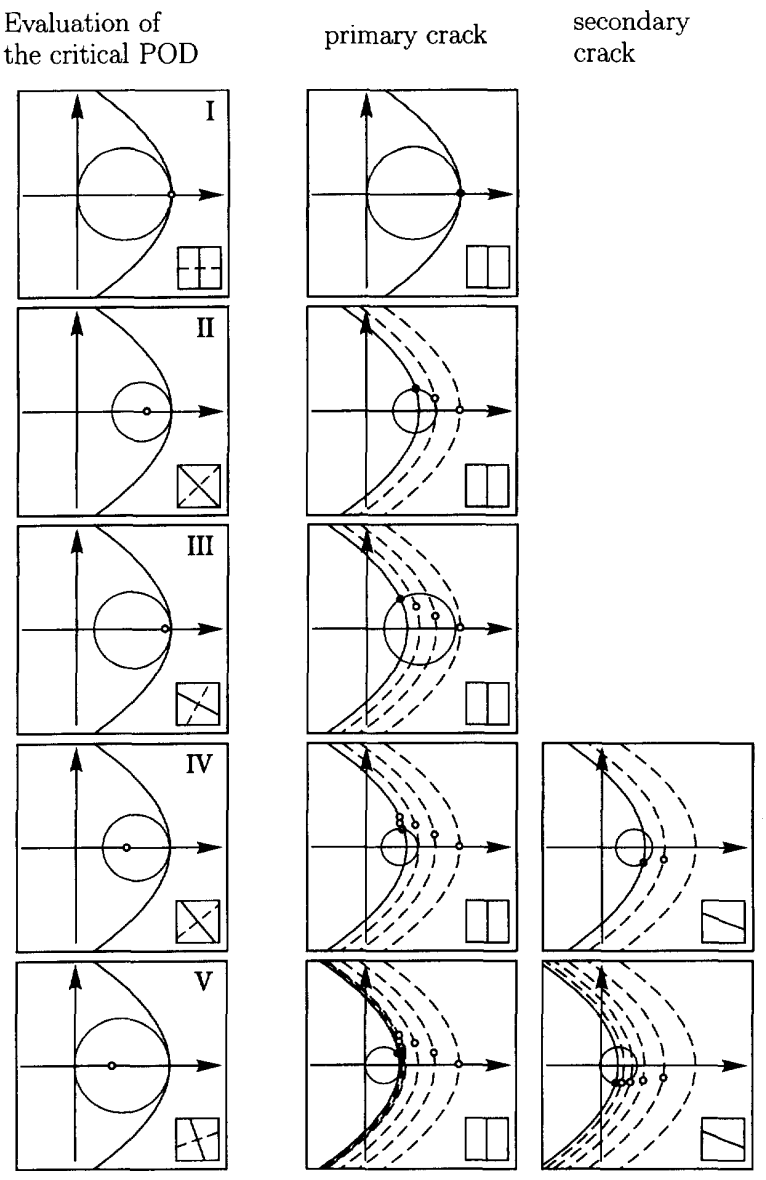

Fig. 10. Detailed evolution at the planes of degradation.

I The current tractions violate the fracture criterion $F_0 = 0$ and the primary crack has just been initiated under Mode I conditions (the fracture criterion is violated in the apex, the current direction of the principal stress is orthogonal to the critical POD). The history of this crack will be depicted in the middle column.

II The loading has been further increased under displacement control. The primary crack is active and is softening, which strongly relaxes the tractions. It is seen that the current Mohr circle is no longer tangential to the softened fracture criterion. The critical POD (left column) is significantly inclined with respect to the primary crack, but the loading has not yet achieved a critical intensity ($F < 0$), and a secondary crack is not yet initiated.

III The primary mechanism is continuously softening, but this (anisotropic) process cannot prevent the tractions from attaining a critical level in the critical POD. Shortly after this time instant, a secondary crack will be initiated, again under (local) Mode I conditions.

IV The secondary crack has opened under an inclination of 66.2° with respect to the

primary crack (right column). The newly introduced softening mechanism leads to an elastic unloading in the primary crack. This primary crack is, therefore, deactivated, and only the second crack remains active.

V The secondary crack is softening. Eventually, the primary crack has been reactivated again and both failure mechanisms are contributing simultaneously to the softening response.

As shown in Fig. 11, the ductility of the response has a significant influence on the angle between the primary and secondary (and further) crack(s) for a given structure. Therefore, the relative toughness $\mathscr{Z}$ is introduced. It correlates the potential energy, which is stored in the material (units: J m^{-3}) at the instant of failure initiation (since failure initiation is triggered by a strength criterion), and the dissipated energy during failure (units: J m^{-2}). This "characteristics process zone size" is divided by a characteristic dimension of the structure d_{ch} to obtain the dimensionless relative toughness $\mathscr{Z}$. Its inverse $1/\mathscr{Z}$ has been previously interpreted as structural brittleness number (ACI, 1992).

$$\mathscr{Z} := \frac{E}{1-\nu^2} \cdot \frac{G_f^{\mathrm{I}}}{q_{n,f_0}^2} \cdot \frac{1}{d_{ch}}. \tag{28}$$

The inclination between primary and secondary cracks in dependence of the relative toughness $\mathscr{Z}$ is given in Fig. 12. If the potential energy at failure initiation is sufficient to instantaneously form the free crack surface ($\rightsquigarrow$ brittle material), then the sudden stress relief activates extensive crack shielding, and secondary cracking can occur only perpendicular to the primary crack. An associated flow rule mobilizes additional stresses due to dilatational effects, which lead to a premature secondary cracking. On the other hand, ductile materials ($\mathscr{Z} \gg 10$) do not relieve stresses and consequently do not activate crack shielding. Thus, the rotating applied stresses subsequently violate the PODs in the sense of a rotating crack model ($\rightsquigarrow \Delta\alpha \to 0$) or a plasticity-based crack model (Feenstra and de Borst, 1995).

6. CLASSIFICATION

With the derived criteria, the heuristic assumptions of the conventional models can be reassessed. If a significant rotation of the principal directions of the applied loading is to be expected, the following recommendations for the range of applicability of the conventional models are deduced:

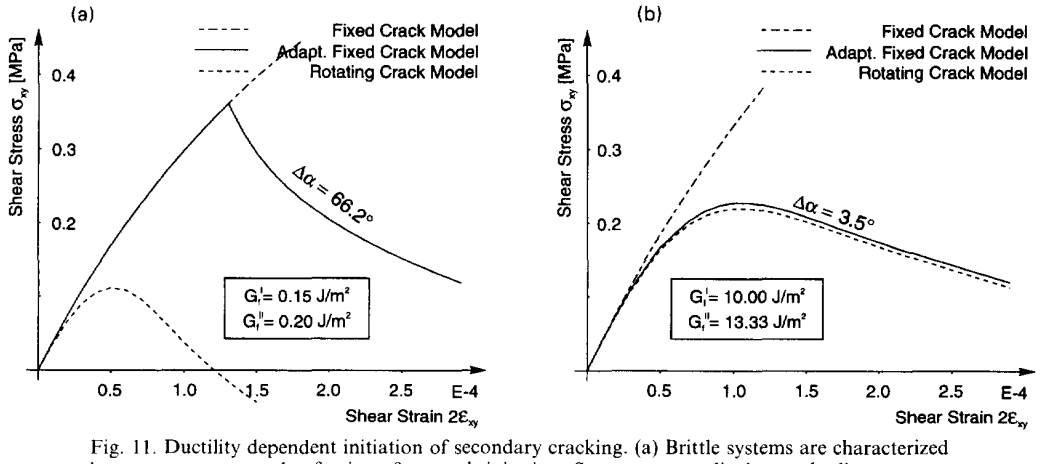

Fig. 11. Ductility dependent initiation of secondary cracking. (a) Brittle systems are characterized by a very pronounced softening after crack initation. Stresses perpendicular to the ligament are relaxed and further cracking is shielded against. Therefore, the applied stress state must rotate significantly before secondary cracking can occur. (b) Ductile systems do not exhibit an abrupt loss of strength, the stress relaxation is not pronounced. Hence, the critical stress state can be exceeded in the vicinity of the initial crack as well and secondary failure can occur at only a slight inclination to the primary 'crack'.

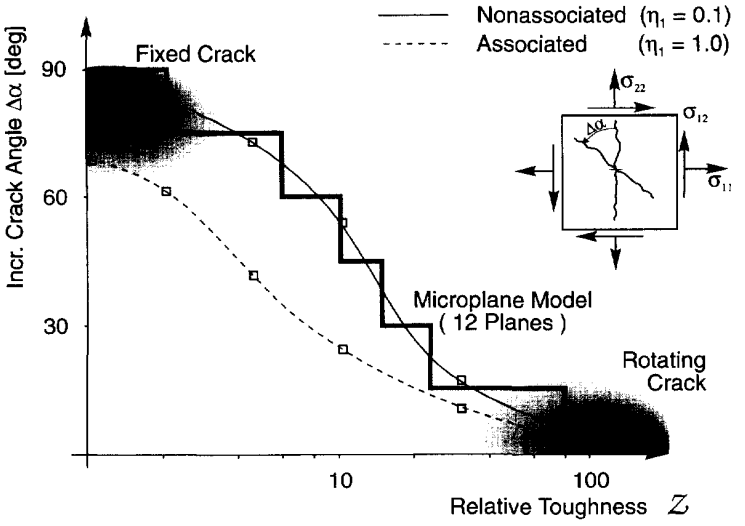

Fig. 12. Angle $\Delta\alpha$ between primary and secondary crack in the tension–shear problem: predictions by the present approach and comparison with the classical models.

(i) The fixed, multiple fixed and rotating crack model assume crack initiation under Mode I. This has been shown to be a valid assumption for materials with a high relative shear strength γ_0 under tensile loading situations [eqn (23)]. Such materials typically exhibit a relatively brittle failure behaviour (e.g. concrete or ceramics).

(ii) As demonstrated, the inclination between primary and secondary cracking is substantial for brittle failure, because pronounced unloading causes significant shielding of cracks parallel to existing ones. Since the fixed crack concept does not account for secondary cracking, the multiple fixed crack model with $\Delta\alpha^{Th} \geqslant 45^\circ$ should be preferred in these situations. However, the choice of $\Delta\alpha^{Th}$ remains arbitrary and the results should be assessed carefully.

(iii) The rotating crack concept combines a mechanism for brittle materials (primary crack initiation under Mode I) with a concept that is appropriate for ductile systems (continuous rotation of the material anisotropy). This reflects the situation of normal-sized reinforced concrete structures very well. The crack initiation itself is very much controlled by the concrete, whereas the crack opening and the degradation of the structural composite is dominated by the ductile behaviour of the steel. For other materials, however, the performance of the RCM is very difficult to assess. It seems to be advantageous in relatively ductile environments, and in this field, it is competing with classical plasticity. For the simulation of failure processes in quasi-brittle materials, it should be used with care.

(iv) The statically constrained microplane model accounts for a proper interaction of normal and shear components. However, a strong dependence of the results on the number of sampling directions is observed, especially if the material is not perfectly brittle, but exhibits some significant toughness. The results converge to the analytical solution given by eqn (21) as the number of sample directions is increased. For this case, however, the numerical treatment is very inefficient and the determination of the active set of cracks becomes extremely difficult.

The proposed adaptive fixed crack model yields consistent results for primary and secondary cracking in the complete range of failure, from perfectly brittle to ductile behaviour. Except for highly ductile situations, where classical plasticity is to be preferred for numerical reasons, the present approach is an attractive enhancement to the conventional fictitious crack models.

7. SUMMARY AND CONCLUSIONS

A generic concept of the smeared crack approach is presented in order to allow for a comprehensive discussion. The abstract notion of a plane of degradation (POD) allows for

the decomposition of the material degradation into the underlying physical phenomena of fracture and its geometrical embedment into the continuum space.

The constitutive description of the cracking mechanism of the POD is the basic ingredient of any fictitious crack model. A formulation with independent softening laws for the normal and shear strength has been presented. It allows for an independent calibration with respect to Mode I and Mode II failure and thus ensures a proper treatment of complex mixed mode situation.

The analytical determination of the orientation of the crack plane yields a unique criterion for the initiation of primary and secondary cracking. It has been emphasized that cracks do not necessarily occur under Mode I conditions, and that the crack orientation is entirely defined by the characteristic strength parameters of the material and the type of the applied loading.

7.1. *Systematic classification of the conventional approaches*

On the basis of the analytical criterion for crack initiation, the heuristic assumptions of the conventional models have been reassessed. Recommendations for the range of applicability of the conventional models has been given depending on the physical characteristic of the material in the structural context, which is under consideration.

7.2. *Unified fictitious crack concept*

The variety of underlying heuristic assumptions of the conventional approaches can be replaced by a unique, analytically based criterion. A unified concept, the adaptive fixed crack model (AFCM) is proposed, in which the overall material behaviour is based solely on the constitutive relations in the failure planes without any additional presuppositions. The adaptive fixed crack model yields consistent results for primary and secondary cracking in the complete range from brittle to ductile response and constitutes an attractive enhancement to the conventional fictitious crack models.

Acknowledgements—The first two authors acknowledge the support of the Deutsche Forschungsgemeinschaft DFG within the Collaborative Research Centre SFB 381. The third author gratefully acknowledges the financial support related to the Max-Planck Research Award given to him by the Max-Planck Society and the Alexander von Humboldt Foundation.

REFERENCES

ACI Committee 466, Fracture Mechanics (1992) Fracture mechanics of concrete: concepts, models and determination of material properties. *International Conference on Fracture Mechanics of Concrete Structures FRAMCOS* 1, ed. Z. P. Bažant, pp. 3–140. Breckenridge, CO. Elsevier, London.

Armero, F. and Garikipati, K. (1996) An analysis of strong discontinuities in multiplicative finite strain plasticity and their relation with the numerical simulation of strain localization in solids. *International Journal of Solids and Structures* **33**(20–22), 2863–2885.

Barenblatt, G. I. (1962) The mathematical theory of equilibrium cracks in brittle fracture. *Advances in Applied Mechanics* **7**, 55–129.

Batdorf, S. B. and Budiansky, B. (1949) A mathematical theory of plasticity based on the concept of slip. Tech. report 1871. National Advisory Committee for Aeronautics (NACA), Washington D.C.

Bažant, Z. P. (1976) Instability, ductility and size effect in strain-softening concrete. *Journal of Engineering Mechanics, ASCE* **102**(EM2), 331–344.

Bažant, Z. P. (1983) Comment on orthotropic models for concrete and geomaterials. *Journal of Engineering Mechanics, ASCE* **109**(3), 849–865.

Bažant, Z. P. (1984) Size effect in blunt fracture: concrete, rock, metal. *Journal of Engineering Mechanics, ASCE* **110**(4), 518–535.

Bažant, Z. P. and Cedolin, L. (1979) Blunt crack band propagation in finite element analysis. *Journal of the Structural Division, ASCE* **105**(2), 297–315.

Bažant, Z. P. and Gambarova, P. (1980) Rough cracks in reinforced concrete. *Journal of the Structural Division, ASCE* **106**(ST4), 819–842.

Carol, I. and Prat, P. C. (1990) A statically constrained microplane model for the smeared analysis of concrete cracking. *International Conference on Computer Aided Analysis and Design of Concrete Structures*, Vol. 2, pp. 919–930.

Carol, I., Bažant, Z. P. and Prat, P. C. (1992) Microplane-type constitutive models for distributed damage and localized cracking in concrete structures. *International Conference on Fracture Mechanics of Concrete Structures FRAMCOS* 1, ed. Z. P. Bažant, pp. 299–304.

Cervenka, V. (1970) Inelastic finite element analysis of reinforced concrete panels under in-plane loads. Ph.D. thesis, University of Colorado, Boulder, CO.

Cope, R. J., Rao, P. V., Clark, L. A. and Norris, P. (1980) Modelling of reinforced concrete behaviour for finite element analysis of bridge slabs. *Numerical Methods for Nonlinear Problems I*, ed. Taylor *et al.*, pp. 457–470.

Coulomb, C. A. (1776) Essai sur une application des règles de maximis et minimis à quelques problèmes de statique, relatifs à l'architecture. *Mémoires de mathematique et de physique* **7,** 343–382.

de Borst, R. and Nauta, P. (1985) Non-orthogonal cracks in a smeared finite element model. *Engineering Computations* **2,** 35–46.

de Borst, R., Sluys, L. J., Mühlhaus, H. B. and Pamin, J. (1993) Fundamental issues in finite element analysis of localization of deformation. *Engineering Computations* **10,** 99–121.

Dugdale, D. S. (1960) Yielding of steel sheets containing slits. *Journal of the Mechanics and Physics of Solids* **8,** 100–104.

Feenstra, P. H. (1993) Computational aspects of biaxial stress in plain and reinforced concrete. Ph.D. thesis, Delft University of Technology (NL).

Feenstra, P. H. and de Borst, R. (1995) Plasticity model and algorithm for Mode-I cracking in concrete. *International Journal for Numerical Methods in Engineering* **38**(15), 2509–2529.

Hillerborg, A., Modéer, M. and Petersson, P. E. (1976) Analysis of crack formation and crack growth in concrete by means of fracture mechanics and finite elements. *Cement and Concrete Research* **6,** 773–782.

Kupfer, H. (1973) Das Verhalten des Betons unter mehrachsiger Kurzzeitbelastung unter besonderer Berücksichtigung der zweiachsigen Beanspruchung. *Deutscher Ausschuß für Stahlbeton*, Vol. 229.

Larsson, R. and Runesson, K. (1996) Element-embedded localization band based on regularized displacement discontinuity. *Journal of Engineering Mechanics, ASCE* **122**(5), 402–411.

Leon, A. (1935) Über die Scherfestigkeit des Betons. *Beton und Eisen* **34**(8), 130–135.

Lin, C. S. and Scordelis, A. C. (1975) Nonlinear analysis of RC shells of general forms. *Journal of the Structural Division, ASCE* **101,** 523–538.

Litton, R. W. (1976) A contribution to the analysis of concrete structures under cyclic loading. Ph.D. thesis, University of California, Berkeley, CA.

Mohr, O. (1906) *Abhandlungen aus dem Gebiete der Technischen Mechanik*, 1st edn. Wilhelm Ernst und Sohn, Berlin.

Oliver, J. (1989) A consistent characteristic length for smeared cracking models. *International Journal for Numerical Methods in Engineering* **28,** 461–474.

Rashid, Y. R. (1968) Ultimate strength analysis of prestressed concrete pressure vessels. *Nuclear Engineering and Design* **7,** 334–344.

Rinderknecht, S. (1994) Delamination in Faserverbundplatten—Ein vereinfachtes Berechnungsmodell. Doctoral thesis, University of Stuttgart (D).

Roš, M. and Eichinger, A. (1949) Die Bruchgefahr fester Körper. Tech. report 172. Eidg. Materialprüfungs- und Versuchsanstalt für Industrie, Bauwesen und Gewerbe EMPA, Zürich.

Rots, J. G. (1988) Computational modeling of concrete fracture. Ph.D. thesis, Delft University of Technology (NL).

Rots, J. G. and de Borst, R. (1987) Analysis of mixed-mode fracture in concrete. *Journal of Engineering Mechanics, ASCE* **113**(11), 1739–1758.

Scanlon, A. (1971) Time dependent deflections of reinforced concrete slabs. Ph.D. thesis, University of Alberta, Edmonton (Canada).

Simo, J. C. and Oliver, J. (1994) A new approach to the analysis and simulation of strain softening in solids. *Fracture and Damage in Quasibrittle Structures*. Prag (CS): E&FN Spon, London.

Stankowski, T. (1990) Numerical simulation of progressive failure in particle composites. Ph.D. thesis, University of Colorado, Boulder, CO.

Suidan, M. and Schnobrich, W. C. (1973) Finite element analysis of reinforced concrete. *Journal of the Structural Division, ASCE* **99**(10), 2109–2122.

Taylor, G. I. (1938) Plastic strain in metals. *Journal of the Institute of Metals* **62,** 307–324.

Weihe, S. (1995) Modelle der fiktiven Rißbildung zur Berechnung der Initierung und Ausbreitung von Rissen: Ein Ansatz zur Klassifizierung. Doctoral thesis, University of Stuttgart (D).

Weihe, S. (1997) Failure induced anisotropy in the framework of multi-surface plasticity. *International Conference on Computational Plasticity, COMPLAS* 5, ed. Owen *et al.*, pp. 1049–1056.

Weihe, S., König, M. and Kröplin, B. (1994) A treatment of mixed mode fracture in debonding. *Computational Materials Science* **3,** 254–262.

Willam, K. J., Pramono, E. and Sture, S. (1987) Fundamental issues of smeared crack models. *SEM/RILEM International Conference on Fracture of Concrete and Rock*, eds. S. P. Shah and S. E. Swartz, pp. 142–153.